catalysts

MDPI

Article

Sol-Gel-Assisted Microwave-Derived Synthesis of Anatase Ag/TiO_2/GO Nanohybrids toward Efficient Visible Light Phenol Degradation

E. H. Alsharaeh [1,*], T. Bora [2], A. Soliman [1,3], Faheem Ahmed [1], G. Bharath [1], M. G. Ghoniem [4], Khalid M. Abu-Salah [5] and J. Dutta [6,*]

1 Department of Chemistry, College of Science and General Studies, Alfaisal University, P.O. BOX 50927, Riyadh 11533, Saudi Arabia; asoliman@alfaisal.edu (A.S.); faheem030@gmail.com (F.A.); sribharath7@gmail.com (G.B.)
2 Center of Excellence in Nanotechnology, Asian Institute of Technology, P.O. Box 4, Klong Luang, Pathumthani - 12120, Thailand; tanujjal@squ.edu.om
3 Physical Chemistry Dept., National Research Centre, Dokki, Cairo 12622, Egypt
4 Department of Chemistry, Faculty of Science, Al-Imam Mohammed ibn Saud University, P.O. BOX 90950, Riyadh 11623, Saudi Arabia; mghoniem1@gmail.com
5 Department of Nanomedicine, King Abdullah International Medical Research Center, King Abdulaziz Medical City, National Guard Health Affairs, P.O. Box 22490, Riyadh 11462, Saudi Arabia; abu-salahkh@ngha.med.sa
6 Functional Materials Division, School of Information and Communication Technology, KTH Royal Institute of Technology, Isafjorsgatan 22, SE-164 40 Kista, Sweden
* Correspondence: ealsharaeh@alfaisal.edu (E.H.A.); joydeep@kth.se (J.D.); Tel./Fax: +966-215-7739

Academic Editor: Damien P. Debecker
Received: 13 March 2017; Accepted: 27 April 2017; Published: 1 May 2017

Abstract: A simple microwave-assisted (MWI) wet chemical route to synthesize pure anatase phase titanium dioxide (TiO_2) nanoparticles (NPs) is reported here using titanium tetrachloride ($TiCl_4$) as starting material. The as-prepared TiO_2 NPs were characterized by electron microscopy, X-ray diffraction, UV/visible absorption spectroscopy, and infrared and Raman spectroscopic techniques. Further modification of the anatase TiO_2 NPs was carried out by incorporating plasmonic silver (Ag) NPs and graphene oxide (GO) in order to enhance the visible light absorption. The photocatalytic activities of the anatase TiO_2, Ag/TiO_2, and Ag/TiO_2/GO nanocomposites were evaluated under both ultraviolet (UV) and visible light irradiation using phenol as a model contaminant. The presence of Ag NPs was found to play a significant role to define the photocatalytic activity of the Ag/TiO_2/GO nanocomposite. It was found that the Ag performed like a sink under UV excitation and stored photo-generated electrons from TiO_2, whereas, under visible light excitation, the Ag acted as a photosensitizer enhancing the photocatalytic activity of the nanocomposite. The detailed mechanism was studied based on photocatalytic activities of Ag/TiO_2/GO nanocomposites. Therefore, the as-prepared Ag/TiO_2/GO nanocomposite was used as photocatalytic materials under both UV and visible light irradiation toward degradation of organic molecules.

Keywords: TiO_2; graphene oxide; XRD; photocatalysts

1. Introduction

The application of titanium dioxide (TiO_2) nanostructures as a photocatalyst material has been extensively investigated for efficient photocatalytic degradation of various organic contaminants, microbes, and viruses due to its excellent chemical stability, physical, optical, and electrical properties [1,2]. TiO_2 exists in three crystallographic forms, namely anatase, rutile, and brookite, where both anatase and rutile forms have tetragonal crystalline structure (with dipyramidal and prismatic habits,

respectively) and the brookite form shows orthorhombic crystalline structure [3]. Among these three forms, anatase TiO_2 have shown highest photocatalytic activity due to its more negative conduction band edge potential, which allows for the generation of more potential energy electrons upon photoexcitation [4,5]. Moreover, compared to the rutile and brookite forms, the anatase form also shows greater crystallinity (hence lower defects), a greater specific surface area, and greater photostability and non-toxicity [5].

In order to prepare TiO_2 nanostructures, several synthesis routes have been explored, such as microwave-assisted synthesis routes, sol-gel processes, the hydrothermal process, direct oxidation, anodization, and physical/chemical vapor deposition techniques [6,7]. Among these various methods, microwave-assisted synthesis routes have attained significant consideration, especially for industrial processing, due to their lower time requirement, rapid heat transfer, and selective heating. Various TiO_2 nanomaterials have been prepared using microwave radiation [8–11]. It has been reported that, by using a microwave-assisted hydrothermal technique, colloidal TiO_2 NPs can be prepared in less than 1 h, while it takes almost a day for the conventional hydrothermal method [8]. Although TiO_2 nanostructures have shown excellent photocatalytic activity, their function is mainly limited to the ultraviolet (UV) region due to the wide band gap of TiO_2 (E_g~3.2 eV). To make TiO_2 visible light active, several techniques have been employed [12–14], among which the coupling of TiO_2 with noble metal NPs, such as gold (Au) and silver (Ag), and carbon nanomaterials, such as graphene oxide (GO), have received significant attention recently. The creation of a localized electric field and the optical vibration of surface plasmons in metal NPs allow for absorption in the visible region and hence enhance the photocatalytic activity of the metal-semiconductor composites under visible light [15–17]. Moreover, the application of GO reduces the overall optical bandgap of the nanocomposites and minimizes the electron–hole (e–h) recombination rate, improving the visible light photocatalytic activity of the nanocomposite [18]. Recently, Shah et al. [19] has reported enhanced photocatalytic activity of mesoporous Ag/TiO_2/reduced graphene oxide ternary composites prepared by the solvothermal method. However, the TiO_2 NPs that they reported contained both anatase and rutile phases. In this work, we report a simple microwave-assisted synthesis route for pure anatase phase TiO_2 NPs. The as-obtained NPs were also modified with plasmonic silver (Ag) NPs and graphene oxide (GO) in order to improve the optical absorption in the visible light region and the charge carrier transport. The photocatalytic activities of anatase TiO_2, Ag/TiO_2, and Ag/TiO_2/GO samples were then investigated under UV and visible light irradiation.

2. Results and Discussion

2.1. Nucleation Mechanism

The formation mechanism of TiO_2, Ag/TiO_2, and Ag/TiO_2/GO nanocomposites using CTAB-assisted sol-gel and following the MWI process is represented in Figure 1. The possible growth mechanism of act TiO_2 NPs prepared by the CTAB-assisted sol-gel-derived MWI method with rapid synthesis. Firstly, the surfactant of CTAB was dissolved in double distilled H_2O to produce micelles acting as nanopore structures, and TiO_2 precursor was added to the CTAB-based micelles template in a sol-gel process. Secondly, the mixed solution was transferred for MWI treatment, and the charge effect of electronegative TiO_2 nuclei aggregates were combined with the electropositive CTAB as a structure controlling agent to obtained ultra-fine TiO_2 NPs. Then the sample was calcined at 300 °C for 4 h to remove the micelles of CTAB and to attain the crystalline TiO_2 NPs. The formation mechanism of Ag/TiO_2 is illustrated in Scheme 1. The detailed formation process for the synthesis of Ag/TiO_2 hybrid nanostructure as follows: an appropriate amount of $AgNO_3$ was dissolved in aqueous solution, and as-prepared CTAB-TiO_2 NPs were then added to the above solution. The positively charged Ag^+ ions were adsorbed on the surface of negatively charged CTAB-functionalized TiO_2 NPs due to electrostatic interactions. Further, the hydrazine hydrate used as a reducing agent to reduce Ag^+ ions to metallic Ag on the surfaces of TiO_2 at MWI in the absence of any stabilizer and surfactant resulted in the formation of Ag NPs on the surface of TiO_2 without any crosslinking agents. Meanwhile, the same synthesis procedure was followed for the preparation of Ag/TiO_2/GO. For these

ternary nanocomposites, GO was prepared by the oxidation of graphite according to a modified Hummers' method and then uniformly dispersed in distilled water. Consequently, the GO solution was added to the CTAB solution and TiO_2 precursor was then added gradually. The Ti^{4+} ions were electrostatically adsorbed with the negatively charged oxygen groups (epoxy, carboxylic, and hydroxyl) of GO sheets [20]. Meanwhile, Ag^+ ions were selectively attached to the residual functional groups of TiO_2/GO nanocomposites and were reduced by hydrazine hydrate, so metallic Ag and TiO_2 NPs were uniformly dispersed on the surface of the GO sheets. The physico-chemical and photochemical properties of the as-prepared samples were further studied using various analytical techniques.

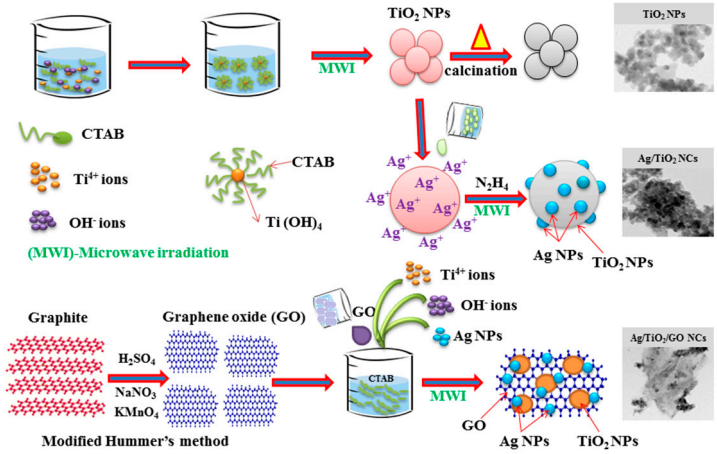

Figure 1. Schematic diagrams of the formation mechanism of TiO_2, Ag/TiO_2, and Ag/TiO_2/GO nanocomposite synthesis by CTAB-assisted sol-gel and MWI techniques.

2.2. Structural and Morphological Analysis

Transmission electron microscopy (TEM) was used to study the morphology of the TiO_2 NPs. Figure 2a shows typical TEM micrographs of the as-prepared TiO_2 NPs along with their size distribution in Figure 2b. To determine the size and shape of the NPs, TEM images from randomly chosen areas of the TEM grid were analyzed by ImageJ software and that way more than 100 particles were analyzed, where the majority of the NPs showed their sizes in between 10 to 13 nm. X-ray diffraction technique studied the crystallinity of the TiO_2 NPs. Figure 2c shows the XRD pattern of the as-prepared TiO_2 NPs. The NPs showed strong X-ray diffraction peaks of (101), (004), (200), (105), (211), (204), (116), (220), and (215) crystal planes representing the anatase phase of TiO_2 confirmed from JCPDS card no. 01-075-2550. No X-ray diffraction peaks from other phases and impurities were observed, indicating the formation of pure anatase phase TiO_2 NPs. The XRD pattern of Ag/TiO_2 confirms the formation of dual phases including the anatase phase of TiO_2 and the face centered cubic (FCC) lattice of Ag. The Ag exhibits 4 major peaks at 2θ values of 38.21, 44.23, 63.1, and 77.31 degrees, assigned to the corresponding 111, 200, 220, and 311 indices, respectively. Moreover, in the XRD pattern of Ag/TiO_2/GO nanocomposite shows dual phases of TiO_2 and Ag, and the peaks of GO vanish due to the high crystalline nature of TiO_2.

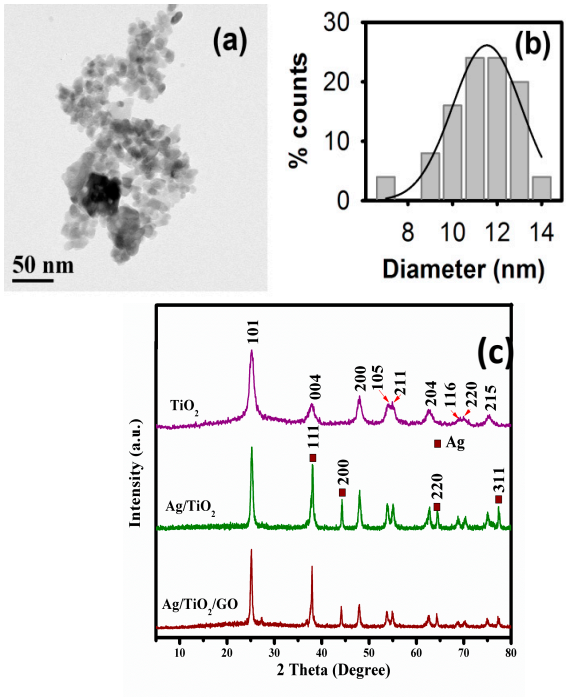

Figure 2. (**a**) TEM micrograph and (**b**) size distribution of TiO_2 NPs prepared using microwave radiation. (**c**) The XRD pattern of the TiO_2, Ag/TiO_2, and Ag/TiO_2/GO nanocomposites showing the crystal planes of the anatase form confirmed from JCPDS 01-075-2550.

The TiO_2 NPs were then coupled with Ag and GO in order to improve the visible light absorption of the samples. Figure 3 shows the typical TEM micrographs of Ag/TiO_2 (Figure 3a) and Ag/TiO_2/GO (Figure 3b) samples along with their UV/visible optical absorption spectra. The anatase TiO_2 NPs showed strong absorption in the UV region and almost no absorption in the visible region beyond 350 nm due to its wide bandgap. Upon incorporation of the Ag NPs, a significant red shift of the optical absorption spectrum towards the visible region was observed, which was mainly due to the surface plasmon resonance (SPR) absorption of the Ag NPs. Additionally, such enhancement in the optical absorption of Ag/TiO_2 nanocomposites was also attributed to the drastic change in the dielectric constant of the surrounding medium due to the presence of Ag NPs.

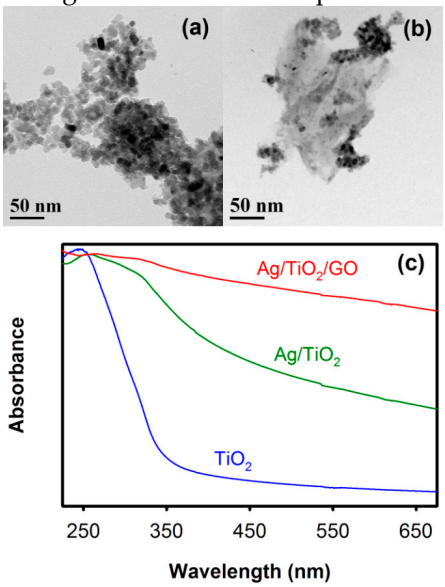

Figure 3. TEM micrographs of (**a**) Ag/TiO_2 and (**b**) Ag/TiO_2/GO samples. (**c**) UV/visible optical absorption spectra of TiO_2, Ag/TiO_2, and Ag/TiO_2/GO samples in water (concentration: 0.1 g/L).

In the case of the Ag/TiO_2/GO nanocomposites, the optical absorption was observed to increase further in the visible region, indicating the reduction in the optical bandgap of the composites. In this regard, it has been reported that GO, which retains the lamellar structure of graphite, contains several unpaired π-electrons that can bond to the free electrons at the surface of TiO_2, resulting in an upward shift of the valance band edge through the formation of Ti–O–C bonds [21,22]. As a result, the overall optical bandgap of the nanocomposite is reduced, making them active under visible light. Figure 4a shows the FTIR spectra of the TiO_2, Ag/TiO_2, and Ag/TiO_2/GO nanocomposites prepared using microwave irradiation. The peaks near 650 cm^{-1} and 1400 cm^{-1} are assigned to the lattice vibration of TiO_2 (Ti–O–Ti stretching). OH bending and stretching modes, observed at 1627 cm^{-1} and 3380 cm^{-1}, indicate the surface adsorbed OH groups or water molecules [15]. Upon incorporation of 10% Ag, the TiO_2 lattice vibration was observed to shift from 1400 cm^{-1} to 1335 cm^{-1}, indicating the formation of Ag–TiO_2 bonding. With 10% GO, the sample showed additional small IR absorption peaks at 1057, 1168, 1230, and 1374 cm^{-1} (shown in inset) related to the C–O, C–OH, and COO–stretching in GO. The intensities of these peaks from GO are relatively very weak due to the possible compound formation between TiO_2 and GO [22]. Figure 4b shows the Raman spectra of the TiO_2, Ag/TiO_2, and Ag/TiO_2/GO samples. The TiO_2 NPs demonstrated a strong Raman band at 144 cm^{-1}, which could be assigned to the E_g optical Raman mode of anatase TiO_2. Other Raman bands observed at 397 cm^{-1}, 516 cm^{-1}, and 638 cm^{-1} were associated with the $B1_g$, $A1_g$, and E_g Raman modes of anatase TiO_2, respectively. In the case of the Ag/TiO_2 nanocomposites, all the Raman bands of the TiO_2 were observed, while no Raman active band from Ag was observed due to the crystal symmetry of Ag. For the Ag/TiO_2/GO nanocomposites, D and G bands from GO were observed at 1347 cm^{-1} and 1604 cm^{-1}, respectively. The E_g mode of TiO_2 was also observed to shift from 144 cm^{-1} to 148 cm^{-1} (shown in inset) due to the interaction of the metal atoms in TiO_2 with the GO layers.

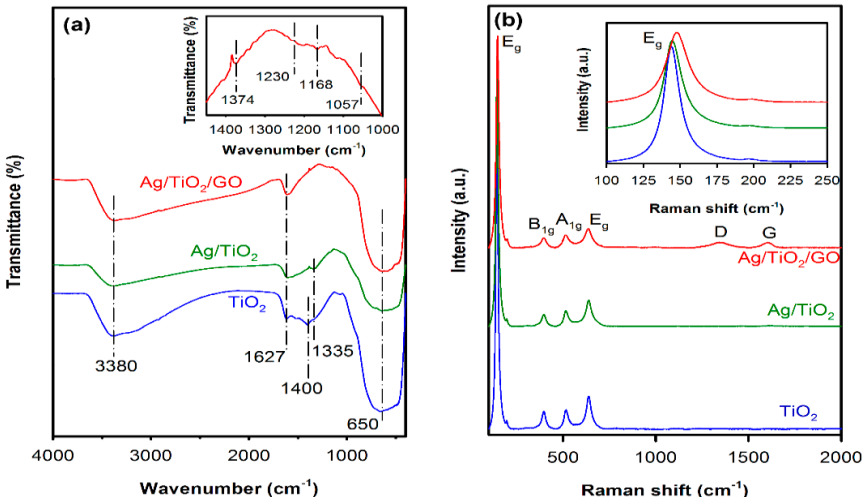

Figure 4. (**a**) FTIR and (**b**) Raman spectra of TiO_2, Ag/TiO_2, and Ag/TiO_2/GO nanocomposites. Inset in (**a**) shows the magnified FTIR spectrum of Ag/TiO2/GO nanocomposites from 1000 to 1450 cm^{-1}, whereas inset in (**b**) shows the magnified Raman spectrum from 100 to 250 cm^{-1}, showing the shift in E_g mode of TiO_2 upon incorporation of GO.

2.3. Photocatalytic Properties

The TiO_2, Ag/TiO_2, and Ag/TiO_2/GO samples were then used to study the photocatalytic activities of the composites under both UV and visible light irradiation. Figure 5 shows the photocatalytic degradation of 10 ppm phenol in aqueous solution using TiO_2, Ag/TiO_2, and Ag/TiO_2/GO nanocomposites as photocatalysts. Under UV irradiation, TiO_2 NPs showed the degradation of phenol with a rate constant of 2.63×10^{-2} min^{-1}, which was almost two times faster than the photolysis of phenol when no photocatalysts were used. The photocatalytic activity of TiO_2 under UV irradiation can be attributed to the high UV absorption by TiO_2 NPs, as observed in Figure

3c. However, when visible light was used, TiO_2 NPs did not show any significant degradation of phenol (Figure 5(b)) due to its low absorption of light in the visible spectrum.

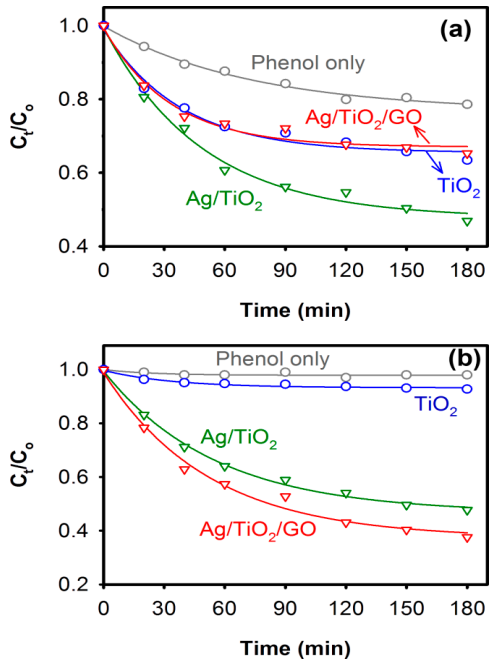

Figure 5. Photocatalytic degradation of 10 ppm phenol in aqueous solution under (**a**) UV and (**b**) visible light irradiation when TiO_2, Ag/TiO_2, and Ag/TiO_2/GO nanocomposites were used as photocatalysts.

In the case of the Ag/TiO_2 nanocomposites, the photocatalytic degradation of phenol was observed to enhance significantly under both UV and visible light irradiation. With UV light, the Ag/TiO_2 nanocomposite showed almost 50% reductions in phenol concentration in 2.5 h. The enhancement was even greater when visible light was used, showing nearly 50% reductions in phenol concentration in 1.5 h. In this regard, it has been reported that the incorporation of metal NPs, such as gold (Au) and silver (Ag) into the semiconductor-based photocatalysts, brings drastic improvement in their photocatalytic activity under both UV and visible light, owing to the several advantages offered by the metal/semiconductor composites, such as enhanced light harvesting due to the localized SPR effect from the metal NPs, a reduced e–h pair diffusion length, an efficient photo-generated charge separation and transfer, and a localized heating effect from metal NPs [16,23]. Upon the incorporation of Ag, a space charge region in the TiO_2 side is created near the metal/semiconductor interface, which upon photo-excitation would force the electrons and holes to move in different directions once they are created, suppressing the e–h pair recombination [24] and thereby improving the overall photocatalytic activity of the nanocomposite. The Ag/TiO_2/GO nanocomposites, on the other hand, showed interesting behavior in their photocatalytic activities. Under UV light irradiation, the photocatalytic activity of the Ag/TiO_2/GO nanocomposite was observed to diminish compared to the Ag/TiO_2 nanocomposite and showed activity very similar to that of the TiO_2 NPs. Improved efficiency in the photocatalytic activity of metal oxide NPs with GO has been reported by several researchers, showing enhanced photo-generated charge separation efficiency [25,26]. However, in the presence of Ag NPs, the photo-generated charge transfer process occurs in a complex manner, as shown in Figure 6a, where Ag NPs act as a sink that can store and shuttle photo-generated electrons back to TiO_2 NPs, limiting the direct charge transfer from UV-excited TiO_2 to GO. Similar capturing of photo-generated electrons by metal NPs and shuttling them back to the semiconductor was also reported previously by our group in the gold–zinc oxide system [27]. As a result, the overall photocatalytic activity of the Ag/TiO_2/GO nanocomposites decreases under UV light irradiation.

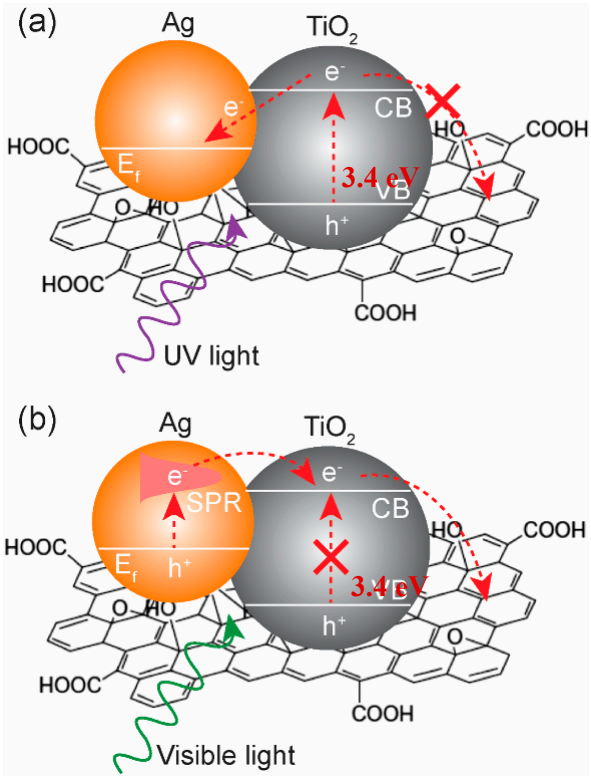

Figure 6. Schematic representation of possible electron transfer paths in Ag/TiO_2/GO nanocomposites under (**a**) UV and (**b**) visible light excitation.

Under the visible light excitation, the e–h pair generation in TiO_2 is limited due to the wide bandgap of the material, while Ag NPs act as photosensitizers, in this case, harvesting the visible light and injecting excited electrons to the conduction band (CB) of TiO_2 from which these electrons can be efficiently captured by GO. The possible photo-generated electron transfer mechanism under visible light irradiation in the Ag/TiO_2/GO nanocomposites is shown in Figure 6b. In this situation, the photo-generated electrons and holes are separated efficiently and then actively participate in photocatalytic reactions. As a result, under visible light irradiation, the Ag/TiO_2/GO nanocomposites showed maximum photocatalytic activity, exhibiting a 50% reduction in phenol concentration in about 1.25 h, which was almost 16% higher than that of the Ag/TiO_2 nanocomposites. This shows a photocatalytic enhancement that is significant compared to mesoporous Ag–TiO_2-reduced graphene oxide ternary composites [19].

3. Experimental

3.1. Preparation of TiO_2 NPs

$TiCl_4$, 99.9%, Arcos Organics (22 mL), was added dropwise to a 1 L beaker containing 0.5 g of N-cetyl-N,N,N-trimethyl ammonium bromide (CTAB) and dissolved in 500 mL of ethanol/water co-solvent (1:1 volume ratio). A pale yellow sol was formed and following that a suitable amount (~400 mL) of 25% NH_4OH solution, Merck, Kenilworth, NJ, U.S.A., was added to adjust the pH of the solution to neutral (pH = 7), forming a gel. The gel solution was then introduced to a commercial microwave oven at 50% microwave power (300 W) and was irradiated for 18 min. The obtained TiO_2 NPs were then centrifuged and washed with ethanol and deionized (DI) water several times. Finally, the NPs were calcined in a furnace (NaberTherm, GmbH Bahnhofstr. Lilienthal (Germany)) at 300 °C, where the temperature was increased at a rate of 1 °C/min and kept at 300 °C for 4 h, after which they were naturally cooled to room temperature.

3.2. Preparation of the Ag/TiO_2 Nanocomposite

To prepare the Ag/TiO_2 nanocomposite, a 0.5 M silver nitrate ($AgNO_3$) aqueous solution was added to TiO_2 NPs suspended in deionized (DI) water, where the Ag-to-TiO_2 ratio (Wt/Wt) was fixed at 10%. The $AgNO_3$ was then reduced with 100 µL of 80% hydrazine hydrate (Loba Chemie, Colaba, Mumbai, Maharashtra, India), and the suspension was irradiated with the conventional microwave (50% power) for 12 min. The resulting Ag/TiO_2 nanocomposite was then washed with ethanol and DI water several times and dried at 80 °C overnight. Finally, the Ag/TiO_2 nanocomposite was calcined following the same process described above.

3.3. Preparation of Ag/TiO_2/GO Nanocomposites

GO was initially prepared according to the modified Hummer's method, where 4.5 g of graphite (fine powder extra pure, Merck) were added to 110 mL of 98% H_2SO_4 (95–98%, Basic) containing 2.5 g of $NaNO_3$ (99.5%, Merck). The solution was then left in an ice bath for 20 min at 0 °C, after which 15 g of $KMnO_4$ was gradually introduced to the mixture maintaining a temperature at 0 °C with vigorous stirring. The mixture was then kept at 40 °C for 2 h with vigorous stirring. After 2 h, the color of the mixture turned to dark green. At this point, 230 mL of DI water was gradually added to the mixture, keeping the temperature below 50 °C, followed by an addition of 20 mL of H_2O_2 (30%, Merck). The stirring was continued for another 20 min while the color of the mixture turned light yellow. Finally, the mixture was centrifuged at 4000 rpm for 10 min and the process was repeated several times (4–5 times), and the precipitate was washed with 10% HCl and DI water every time to remove the acid and nitrate residues. Finally, a brown paste of GO was obtained, which was then dried at 50 °C overnight. To prepare the Ag/TiO_2/GO nanocomposites, 1.9 g of GO was added to the CTAB solution used for the preparation of TiO_2 NPs, prior to the addition of $TiCl_4$ to it. The atom % of GO-to-TiO_2 was 10% at this point. All other steps were then carried out in the same sequence as mentioned in the previous sections to prepare the TiO_2 NPs first, followed by the deposition of Ag NPs, which finally resulted in the Ag/TiO_2/GO nanocomposite.

3.4. Characterization Techniques

The morphologies of the TiO_2 NPs, and the Ag/TiO_2 and Ag/TiO_2/GO nanocomposites, were characterized by transmission electron microscopy (TEM; Model: JEOL JEM-2100F) at 200 kV. X-ray diffraction (XRD) patterns in the range of 20–75° were recorded by a MiniFlex600 (Rigaku, Tokyo, Japan) X-ray diffractometer using Cu-Kα radiation (wavelength = 1.5406 Å). A Perkin Elmer Lambda 25 UV/Vis spectrometer (Perkin Elmer, Waltham, MA, United States) was used to record the optical absorption spectra, while a Perkin-Elmer Frontier FTIR spectrometer was used to obtain the FTIR spectra of the samples. FTIR spectra were recorded averaging over 100 scans from 400 to 4000 cm^{-1} at a 4 cm^{-1} resolution. A confocal Raman microscope (XploRA ONE from Horiba, Kyoto, Japan) was used to obtain the Raman spectra of the samples. Raman spectra were collected from 100 to 2000 cm^{-1} using 532 nm laser excitation (25 mW) along with a 20 s integration time, a 1800 gr/mm grating with a spectral resolution better than 2 cm^{-1}, and all measurements were recorded at room temperature.

3.5. Photocatalytic Tests

A 10 ppm phenol solution was prepared in DI water and used as a model contaminant to study the photocatalytic activity of TiO_2, Ag/TiO_2, and Ag/TiO_2/GO nanocomposites. Three milliliters of phenol solution was added to 3 separate quartz cuvettes to which TiO_2, Ag/TiO_2, and Ag/TiO_2/GO nanocomposites were added. The concentration of photocatalysts in all cases was maintained at 0.1 g/L. The cuvettes were then kept in darkness for 2 h under slow stirring in order to achieve an adsorption/desorption equilibrium between the photocatalysts and phenol. After 2 h, the cuvettes were placed under the illumination of 254 nm (UV) radiation, (3UVTM 36-lamp (6 Watts), UVP, LLC) with constant stirring. For visible light excitation, cuvettes, after attaining the adsorption/desorption equilibrium, were placed under simulated solar light (AM 1.5G radiation, 1 kW/m^2) that was obtained

from a solar simulator (SS1.6 kW from Sciencetech, ON, Canada). Photocatalytic degradation of phenol was carried out for 180 min under both UV and visible light irradiation.

Analytical Method for Degradation Assay

To study the degradation kinetics, 20 μL of phenol solution was collected at regular intervals during the photocatalytic tests and concentration of phenol was then measured at every point by using high performance liquid chromatography (HPLC). A co-solvent of methanol with water (a volume ratio of 45:55) with pH 3.0 adjusted by sulfuric acid (H_2SO_4) was used as the mobile phase for the HPLC separation. A flow rate of 1 mL/min was fixed and the HPLC analysis was carried out using a C18 column (5 μm) maintained at room temperature. A Dionex UVD 170S diode array detector set at 245 nm was used for the detection of phenol. The rate of photocatalytic degradation kinetics of phenol plotted as C_t/C_o against both UV and visible light irradiation time, where C_t is the concentration of phenol at irradiation time "t" measured by HPLC, and C_o is the initial concentration of phenol (10 ppm).

4. Conclusions

Pure anatase phase TiO_2 NPs were synthesized using a simple microwave-assisted wet chemical route, where the TiO_2 NPs were successfully decorated with plasmonic Ag nanoparticle and GO to improve the visible light harvesting. The as-prepared TiO_2 NPs showed sizes between 10 and 13 nm, with strong optical absorption in the UV region. The incorporation of Ag and GO further enhanced the optical absorption of the Ag/TiO_2 and Ag/TiO_2/GO nanocomposites. FTIR and Raman analysis revealed the successful interaction of metal ions in TiO_2 with GO, which can lead to the upward shifting of the valance band edge of TiO_2 narrowing the overall optical bandgap of the nanocomposites, resulting in the enhancement of the visible light absorption, which was also partly due to the SPR absorption of Ag NPs. The presence of Ag NPs was found to be crucial for the efficiency of the photocatalytic activity of the nanocomposites. Under UV light, Ag NPs act as a sink and store photo-generated electrons from TiO_2, limiting the direct transfer of excited electrons from TiO_2 to GO and thereby negatively affecting the photocatalytic performance of Ag/TiO_2/GO nanocomposites. However, under visible light irradiation, Ag NPs act like photosensitizers and donate electrons that can be captured effectively to TiO_2 by ensuring enhanced charge separation in the Ag/TiO_2/GO nanocomposites, which leads to an efficient visible light photocatalytic degradation of phenol.

Acknowledgments: This project was funded by King Abdulaziz City for Science and Technology—the Kingdom of Saudi Arabia-award number (AT-35-109). The authors would like to thank the Chair in Nanotechnology, The Research Council of Oman for technical support.

Author Contributions: E.H.A. contributed to the conception and design of the experiments. E.H.A. and A.S carried out all experiments. T.B. performed photoctalysis analyses, characterizations and wrote the paper. G.B. prepared figures and formatted the manuscript and wrote the discussion and growth mechanism. F.A. contributed in analysis of the data and results and discussion part. J.D., K.A., and M.G.G. participated in the scientific discussion during the preparation of this manuscript. All authors reviewed the manuscript.

Conflicts of Interest: The authors declare no conflicts of interest.

References

1. Nakata, K.; Fujishima, A. TiO_2 photocatalysis: Design and applications. *J. Photochem. Photobiol. C Photochem. Rev.* **2012**, *13*, 169.
2. Hajkova, P.; Spatenka, P.; Horsky, J.; Horska, I.; Kolouch, A. Photocatalytic effect of TiO_2 films on viruses and bacteria. *Plasma Processes Polym.* **2007**, *4*, S397.
3. Puma, G.L.; Bono, A.; Krishnaiah, D.; Collin, J.G. Preparation of titanium dioxide photocatalyst loaded onto activated carbon support using chemical vapor deposition: A review paper. *J. Hazard. Mater.* **2008**, *157*, 209.
4. Agrios, H.A.G.; Gray, K.A.; Rajh, T.; Thurnauer, M.C. Anatase TiO_2 nano-needle and heterostructures for Photocatalysis, Electrochemical and Photoelectrochemical applications. *J. Phys. Chem. B* **2003**, *107*, 4545.
5. Macwan, D.P.; Dave, P.N.; Chaturvedi, S. A review on nano-TiO_2 sol–gel type syntheses and its applications. *J. Mater. Sci.* **2011**, *46*, 3669.

6. Chen, X.; Mao, S.S. Titanium dioxide nanomaterials: synthesis, properties, modifications, and applications. *Chem. Rev.* **2007**, *107*, 2891.
7. Gupta, S.M.; Tripathi, M. A review on the synthesis of TiO_2 nanoparticles by solution route. *Cent. Eur. J. Chem.* **2012**, *10*, 279.
8. Corradi, B.; Bondioli, F.; Focher, B.; Ferrari, A.M.; Grippo, C.; Mariani, E.; Villa, C. Conventional and Microwave-Hydrothermal Synthesis of TiO_2 Nanopowders. *J. Am. Ceram. Soc.* **2005**, *88*, 2639.
9. Huang, C.-H.; Yang, Y.-T.; Doong, R.-A. Microwave-assisted hydrothermal synthesis of mesoporous anatase TiO_2 via sol–gel process for dye-sensitized solar cells. *Microporous Mesoporous Mater.* **2011**, *142*, 473.
10. Wang, H.-E.; Zheng, L.-X.; Liu, C.-P.; Liu, Y.-K.; Luan, C.-Y.; Cheng, H.; Li, Y.Y.; Martinu, L.; Zapien, J.A.; Bello, I. Rapid microwave synthesis of porous TiO2 spheres and their applications in dye-sensitized solar cells. *J. Phys. Chem. C* **2011**, *115*, 10419.
11. Cui, L.; Hui, K.N.; Hui, K.S.; Lee, S.K.; Zhou, W.; Wan, Z.P.; Thuc, C.-N.H. Facile microwave-assisted hydrothermal synthesis of TiO_2 nanotubes. *Mater. Lett.* **2012**, *75*, 175.
12. Etacheri, V.; di Valentin, C.; Schneider, J.; Bahnemann, D.; Pillai, S.C. Visible-light activation of TiO_2 photocatalysts: advances in theory and experiments. *J. Photochem. Photobiol. C Photochem. Rev.* **2015**, *25*, 1.
13. Truong, Q.D.; Le, T.H.; Liu, J.Y.; Chung, C.C.; Ling, Y.C. Synthesis of TiO_2 nanoparticles using novel titanium oxalate complex towards visible light-driven photocatalytic reduction of CO_2 to CH_3OH. *Appl. Catal. A Gen.* **2012**, *437*, 28–35.
14. Truong, Q.D.; Liu, J.Y.; Chung, C.C.; Ling, Y.C. Design and fabrication of semiconductor photocatalyst for photocatalytic reduction of CO_2 to solar fuel. *Catal. Commun.* **2012**, *19*, 8589
15. Saoud, K.; Alsoubaihi, R.; Bensalah, N.; Bora, T.; Bertino, M.; Dutta, J. Synthesis of supported silver nanospheres on zinc oxide nanorods for visible light photocatalytic applications. *Mater. Res. Bull.* **2015**, *63*, 134.
16. Bora, T.; Myint, M.T.Z.; Al-Harthi, S.H.; Dutta, Role of surface defects on visible light enabled plasmonic photocatalysis in Au–ZnO nanocatalysts. *J. RSC Adv.* **2015**, *5*, 96670.
17. Bora, T.; Zoepfl, D.; Dutta, J., Importance of plasmonic heating on visible light driven photocatalysis of gold nanoparticle decorated zinc oxide nanorods. *Sci. Rep.* **2016**, *6*, 26913.
18. Mathpal, M.C.; Tripathi, A.K.; Kumar, P.; R, B.; Singh, M.K.; Chung, J.S.; Hur, S.H.; Agarwal, A. Polymorphic transformations and optical properties of graphene-based Ag-doped titania nanostructures. *Phys. Chem. Chem. Phys.* **2014**, *16*, 23874.
19. Shah, M.S.A.S.; Zhang, K.; Park, A.R.; Kim, K.S.; Park, N.-G.; Park, J.H.; Yoo, P.J. Single-step solvothermal synthesis of mesoporous Ag–TiO2–reduced graphene oxide ternary composites with enhanced photocatalytic activity. *Nanoscale* **2013**, *5*, 5093.
20. Garg, B.; Bisht, T.; Ling, Y. Graphene-based nanomaterials as heterogeneous acid catalysts: A comprehensive perspective. *Molecules* **2014**, *19*, 14582–14614.
21. Umrao, S.; Abraham, S.; Theil, F.; Pandey, S.; Ciobota, V.; Shukla, P.K.; Rupp, C.J.; Chakraborty, S.; Ahuja, R.; Popp, J. A possible mechanism for the emergence of an additional band gap due to a Ti–O–C bond in the TiO2–graphene hybrid system for enhanced photodegradation of methylene blue under visible light. *RSC Adv.* **2014**, *4*, 59890.
22. Zhang, Y.; Pan, C. TiO_2/graphene composite from thermal reaction of graphene oxide and its photocatalytic activity in visible light. *J. Mater. Sci.* **2010**, *46*, 2622.
23. Chen, X.; Zhu, H.-Y.; Zhao, J.-C.; Zheng, Z.-F.; Gao, X.-P. Visible-Light-Driven Oxidation of Organic Contaminants in Air with Gold Nanoparticle Catalysts on Oxide Supports. *Angew. Chem. Int. Ed*. **2008**, *120*, 5433.
24. Zhang, X.; Chen, Y.L.; Liu, R.S.; Tsai, D.P. Plasmonic photocatalysis. *Rep. Prog. Phys*. **2013**, *76*, 046401.
25. Yokomizo, Y.; Krishnamurthy, S.; Kamat, P.V. Photoinduced electron charge and discharge of graphene–ZnO nanoparticle assembly. *Catal. Today* **2013**, *199*, 36.
26. Lightcap, V.; Murphy, S.; Schumer, T.; Kamat, P.V., Photoinduced electron charge and discharge of graphene–ZnO nanoparticle assembly. *J. Phys. Chem. Lett*. **2012**, *3*, 1453.
27. Sarkar, S.; Makhal, A.; Bora, T.; Baruah, S.; Dutta, J.; Pal, S.K., Photoselective excited state dynamics in ZnO–Au nanocomposites and their implications in photocatalysis and dye-sensitized solar cells. *Phys. Chem. Chem. Phys.* **2011**, *13*, 12488.